Approximate Bisimulations for Sodium Channel Dynamics

Abhishek Murthy[1], Md. Ariful Islam[1], Ezio Bartocci[2], Elizabeth M. Cherry[5], Flavio H. Fenton[3], James Glimm[4], Scott A. Smolka[1], and Radu Grosu[2]

[1] Department of Computer Science, Stony Brook University
[2] Department of Computer Engineering, Vienna University of Technology
[3] Department of Biomedical Sciences, Cornell University
[4] Department of Applied Mathematics and Statistics, Stony Brook University
[5] School of Mathematical Sciences, Rochester Institute of Technology

Abstract. This paper shows that, in the context of the Iyer et al. 67-variable cardiac myocycte model (IMW), it is possible to replace the detailed 13-state continuous-time MDP model of the sodium-channel dynamics, with a much simpler Hodgkin-Huxley (HH)-like two-state sodium-channel model, while only incurring a bounded approximation error. The technical basis for this result is the construction of an *approximate bisimulation* between the HH and IMW channel models, both of which are input-controlled (voltage in this case) continuous-time Markov chains. The construction of the appropriate approximate bisimulation, as well as the overall result regarding the behavior of this modified IMW model, involves: (1) The identification of the voltage-dependent parameters of the m and h gates in the HH-type channel, via a two-step fitting process, carried out over more than 22,000 representative observational traces of the IMW channel. (2) Proving that the distance between observations of the two channels is bounded. (3) Exploring the sensitivity of the overall IMW model to the HH-type sodium-channel approximation. Our extensive simulation results experimentally validate our findings, for varying IMW-type input stimuli.

1 Introduction

The emergence of high throughput data acquisition equipment has changed cell biology from a purely wet lab-based science to also an engineering and information science. The identification of a mathematical model from cellular experimental data, and the use of this model to predict and control the cell's behavior, are nowadays indispensable tools in cell biology's arsenal [35, 5].

Continual progress in data acquisition has also led to the creation of increasingly sophisticated partial Differential Equations Models (DEMs) for cardiac cells (myocytes). These are similar in spirit to the DEMs used in physics: their main purpose is to elucidate the biological laws governing the electric behavior of cardiac myocytes, i.e., their underlying cellular and ionic processes [9].

Inspired by the squid-neuron DEM [19] developed by Hodgkin and Huxley (HH), Luo and Rudy (LR) devised one of the first myocyte DEMs, for guinea

pig ventricular cells [29]. Adapting this model to human myocytes led to the ten Tusscher-Noble^2-Panfilov (TNNP) DEM [40], which has 17 state variables and 44 parameters. Based on updated experimental data, Iyer, Mazhari and Winslow (IMW) subsequently developed a DEM comprising of 67 state variables and 94 parameters [20]. This DEM reflects a highly detailed physiological view the electrochemical behavior of human myocytes.

From 17 to 67 variables, all such DEMs capture myocytic behavior at a particular level of abstraction, and hence all of them play an important role in the modeling hierarchy. It is essential, however, to maintain focus on the purpose of a particular DEM; that is, of the particular cellular and ionic processes whose behavior the DEM is intended to capture. Disregarding this purpose may lead to the use of unnecessarily complex DEMs, which may render not only analysis, but also simulation, intractable.

If the only entity of interest is the myocyte's transmembrane voltage, co-authors Cherry and Fenton have experimentally shown that a minimal DEM (MM) consisting of only 4 variables and 27 parameters can accurately capture voltage propagation properties in 1D, 2D, and 3D networks of myocytes [4]. The MM has allowed us to obtain dramatic simulation speedups [1], and to use its linear hybridization as the basis for formal symbolic analysis [18].

Since new technological advances are expected to lead to further insights into myocytic behavior, it is likely that the IMW model will be further refined, by adding new variables. As in model checking and controller synthesis, one would therefore like to compute the smallest approximation of the State-Of-the-Art DEM (SOA), which is observationally equivalent to the SOA with respect to the property of interest, modulo some specified approximation error. This, however, is not an easy task, as it implies the automatic approximation of very large nonlinear DEMs.

A first step toward the desired automation is to identify a set of approximation techniques that allow one to systematically remove unobservable variables from, say, the SOA to end up with the MM, if the only observable variable is the voltage. This is one of the goals of the project Computational Modeling and Analysis of Complex Systems (CMACS) [36]. A byproduct of this work is to establish a long-missing formal relation among the existing myocyte DEMs, facilitating the transfer of properties established at one layer of abstraction to the other layers. Building such *towers of abstraction* is becoming increasingly prevalent in systems biology [22, 11].

The main focus of this paper is on *sodium channel approximations*. In the HH DEM and Noble's DEM of [37], the transmembrane sodium channel is assumed to consist of four independent Markovian gates, whose opening and closing rates depend on the transmembrane voltage. The probability of each of the three identical activating (m-type) gates being open, i.e. a state favoring ion flow, is denoted by m, and the probability of the fourth inactivating (h-type) gate being open is denoted by h. The sodium channel conducts when all the four gates are in the open state.

The IMW model uses the formulation of Irvine et al. [28], where experimental data is used to show the existence of five interdependent gates. This leads to a considerably larger Markovian model for the sodium channel, consisting of 13 state variables.

The main question posed in this paper is the following: *assuming that the conductance of the sodium channel is the only observable, is the behavior of the HH channel equivalent to the behavior of the IMW channel, modulo a well-defined approximation error?* Rather than dealing with behavioral equivalence explicitly, we ask if it is possible to construct an approximate bisimulation [12, 14, 13, 15] between the discrete time versions of the HH and the IMW channel models? This notion of equivalence is stronger than the conventional behavioral equivalence, which compares the observed behaviors (trajectories) of two systems. Also, proving the two models to be approximately bisimilar ensures that when the 13-state sodium channel model is replaced by the 2-state HH-type abstraction in the overall IMW cardiac cell model, the modified IMW model retains the properties of interest (in discrete time). Thus the reduced 2-state model is a valid reduction in the context of the whole-cell IMW model. The answer to the above-posed question is of broad interest, as it reduces to showing the existence of an approximate bisimulation between two Continuous-Time Markov Decision Processes (CT-MDPs), that is, two input-controlled (voltage in this case) continuous-time Markov chains (CTMCs). We answer this question in the positive, by explicitly constructing such a bisimulation.

The construction involves: (1) The identification of the voltage-dependent parameters of the m and h-type gates of the HH-type abstraction, based on the observations of the IMW channel. (2) Proving that the distance between the observations of the two channels never exceeds a given error. (3) Exploring the sensitivity of the overall IMW DEM to the HH-type sodium-channel approximation. The identification of the voltage-dependent parameters is performed via a 2-step fitting process. In the first step, which we call *Parameter Estimation from Finite Traces*, more than 22,000 observational traces of the IMW channel are fit to obtain the parameter values at constant voltage. The second stage, which we call *Rate Function Identification*, combines the stage-1 constant-voltage parameter values to obtain the voltage-dependent parameters defining the HH-type channel. Finally, the resulting 2-state HH-type channel is proved to be approximately bisimilar to the IMW channel and the error between the two systems is bounded. See Fig. 1 for an overview of the approach.

The rest of the paper is organized as follows. Section 2 introduces the relevant background for the HH and the IMW DEMs and their sodium-channel MDP formulations. Section 3 presents our parameter identification technique and the resulting HH-type MDP for the sodium channel. Section 4 proves the existence of an approximate bisimulation between the HH and IMW sodium-channel MDPs. Sections 5 and 6 discuss related work, our conclusions, and future directions.

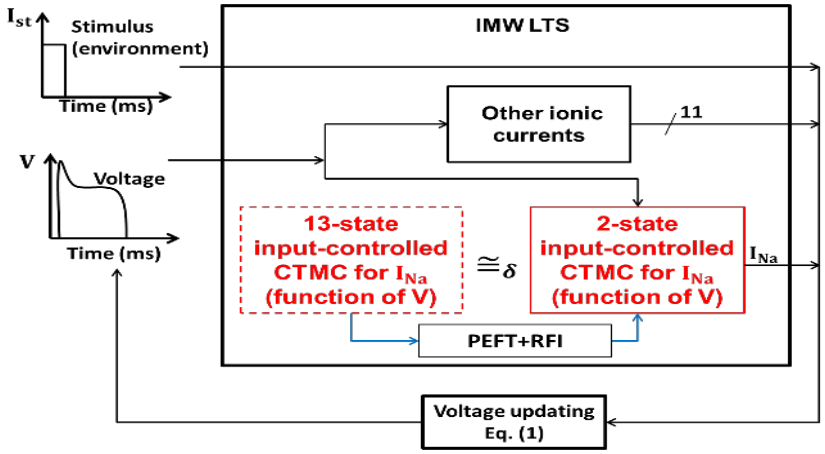

Fig. 1. A Labeled Transition System (LTS)-based view of the IMW DEM, composed of various concurrently evolving subsystems corresponding to the different ionic currents. We replace the 13-state I_{Na} subsystem with a 2-state HH-type abstraction. PEFT and RFI are the two steps of identifying the abstract model. As the 2-state model is proved to be approximately bisimilar (denoted by $\cong_\delta$) to the detailed model, composing it with the other concurrently evolving ionic current models (subsystems) retains the cell-level behaviors of the IMW model. Note that the subsystems ignore the stimulus input during their respective evolution and only depend upon the voltage input. The LTS outputs the 13 currents in Eq. (1).

2 Background

The heart is the central organ of the circulatory system and is responsible for pumping blood in the pulmonary and systemic circulation loops [8]. Pumping is achieved through the synchronized contraction of around four billion myocytes, which constitute the cardiac tissue. This is controlled in a distributed fashion, through the propagation and reinforcement of an electric pulse (clock). The pulse originates in the sino-atrial node of the heart and diffuses from one myocyte to the other through a sophisticated communication infrastructure.

Cardiac myocytes belong to the class of excitable cells, which also includes neurons. Such cells respond to an external electrical stimulus in the form of an Action Potential (AP), which measures the change of the transmembrane potential with time in response to the stimulus. A typical ventricular myocyte AP and its associated phases are shown in Fig. 2(Right). Starting from the resting state, a myocyte can either be excited by an external stimulus or by the diffusing charge of the neighboring myocytes. In this paper, we will restrict our focus on the upstroke phase of the AP.

2.1 The IMW Cellular Model

The IMW DEM is a physiologically detailed model capturing the ionic processes responsible for the generation of an AP in human ventricular myocytes:

$$-C\dot{V} = I_{Na}+I_{Na_b}+I_{Ca}+I_{Ca_b}+I_{K_r}+I_{K_s}+I_{K_1}+I_{to_1}+I_{p(Ca)}+ I_{NaCa}+I_{NaK}+I_{CaK}+I_{st} \quad (1)$$

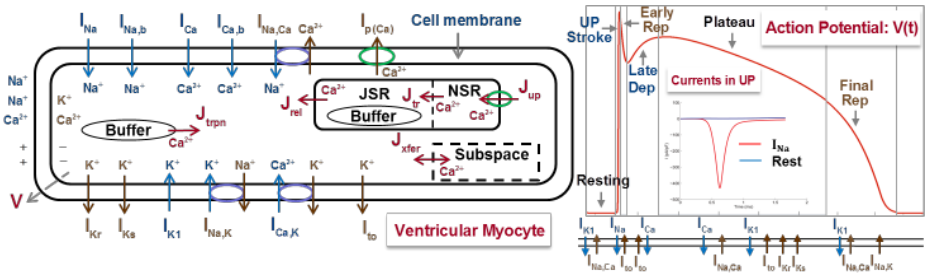

Fig. 2. (Left) Currents in IMW: Blue and brown arrows show ionic currents flowing through channels. Blue circles and arrows correspond to ionic exchanger currents and green circles denote ionic pumps. Intra-cellular currents are shown in Magenta. (Right) The Action Potential (AP), its phases and associated currents. (Right-Inlay) Sodium current in red, and the sum of all other currents in blue, in Upstroke Phase (UP).

where V is the membrane's potential, $\dot{V}$ is its first-order time derivative, C is the membrane's capacitance, and I_v are the ionic currents shown in Fig. 2(Left), except for I_{st}. This is the stimulus current, which could be either an external stimulus or the diffused charge from neighboring cells.

The remaining currents are the result of the flow of the sodium (Na^+), potassium (K^+) and calcium (Ca^{2+}) ions, across the myocyte's membrane. Three types of transport mechanisms are responsible for the ion flows: channels, pumps and exchangers. Channels are special proteins that penetrate the membrane's lipid bi-layer, and are selectively permeable to ions species. Depending on the conformation of the constituent protein, the channel either allows or inhibits the unidirectional movement of an ion specie.

The protein conformation is voltage dependent, thus the name voltage-gated channels. All the transmembrane currents in Fig. 2 result from voltage-gated ionic channels, except for I_{NaK}, I_{NaCa} and $I_{p(Ca)}$, which are exchanger or pump currents. The concentration of calcium is regulated by a sophisticated intracellular mechanism, and is out of scope of this paper.

Fig. 2(Right-inlay) plots the sodium current I_{Na} and the sum of all the other ionic currents during the upstroke phase (UP), of a typical AP of the IMW DEM. The sodium current I_{Na} dominates all the other. *The behavior of the sodium channel, which regulates the flow of I_{Na}, chiefly contributes to the upstroke phase, and will be the focus in the remainder of the paper.* In the HH DEM the situation is similar, and in MM the role of I_{Na} is played by the abstract fast inward current J_{fi}.

2.2 The HH Sodium Current

The sodium current I_{Na} in the HH DEM is defined by the following equation:

$$I_{Na} = \overline{g}_{Na}\, m^3(V)\, h(V)\, (V - V_{Na})$$

where $\overline{g}_{Na}$ is the maximum conductance of the sodium channel, V_{Na} is the sodium's channel Nernst potential, $m(V)$ and $h(V)$ are the probabilities of the voltage-dependent activation gate and the inactivation gates being open respectively.

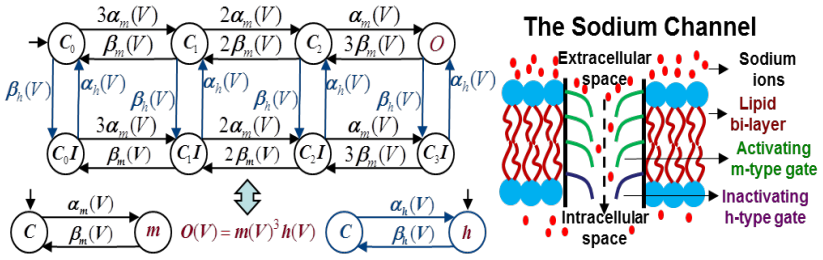

Fig. 3. (Left-top) Sodium channel MDP in 8 states counting the number of independent open/closed gates, and observation function $O(t)$. (Left-bottom) The open-closed MDPs for the m and h-type gates. The equivalent sodium channel behavior is obtained as $O(t) = m(V)^3 h(V)$. (Right) The schematic representation of the sodium channel with its associated independent gates.

A graphic illustration of the sodium channel is given in Fig. 3 (Right). It consists of four independent voltage-controlled gates, three of which are identical activation gates (m-type), and one of which is an inactivation gate (h-type).

The activation and inactivation gates are shown in Fig. 3 (Left-bottom). They are Continuous Time Markov Decision Processes (CT-MDP). Both CT-MDPs have a closed and an open state, respectively, and the rates of transitioning between these two states are given by the voltage-dependent parameters $\alpha(V)$ and $\beta(V)$. The 8-state CT-MDP for the whole channel is shown in the left-half of Fig. 3. Evolution of the state variables (occupancy probabilities of the 8 states) of this model is governed by Kolmogorov equations[21], which form an 8-state DEM. It turns out that any of the 8-variables can be observed using the two gates m and h as they form a stable invariant manifold of the 8-state DEM [23]. At rest the m-gate is closed and the h-gate is open. Their DEM is as follows:

$$\dot{m} = \alpha_m(V)(1-m) - \beta_m(V)m, \qquad \dot{h} = \alpha_h(V)(1-h) - \beta_h(V)h$$

We refer to this DEM as M_H. The linear system obtained by fixing $V = v$ will be denoted as M_H^v. At any point in time the occupancy probability of the open state O in the 8-state DEM is given by $m(V)^3h(V)$. Thus the observation function O of this DEM will be $m(V)^3h(V)$. We now introduce the following notation:

$$x = [m, h]', \quad A = diag(-(\alpha_m + \beta_m), -(\alpha_h + \beta_h)), \quad B = [\alpha_m, \alpha_h]'$$

The independence of the gates also implies that the DEM is in diagonal form, and it can be therefore written as follows:

$$\dot{x} = Ax + B, \qquad x_0 = [m_0, h_0]'$$

Despite the linear-looking form, this equation is nonlinear, as A and B depend on the voltage. For example, Fig. 4(a) shows its numeric solution for the input in Fig. 4(c). However, HH computed an approximate closed form solution as follows. In the resting state, defined as $V = 0$, and in the equilibrium state, for a fixed $V = v$, the gates m and h, and the rates τ have the following values:

$$\begin{array}{ll} m_0 = \alpha_{m_0}/(\alpha_{m_0} + \beta_{m_0}), & m_\infty = \alpha_m/(\alpha_m + \beta_m) \\ h_0 = \alpha_{h_0}/(\alpha_{h_0} + \beta_{h_0}), & h_\infty = \alpha_h/(\alpha_h + \beta_h) \\ \tau_m = 1/(\alpha_m + \beta_m), & \tau_h = 1/(\alpha_h + \beta_h) \end{array}$$

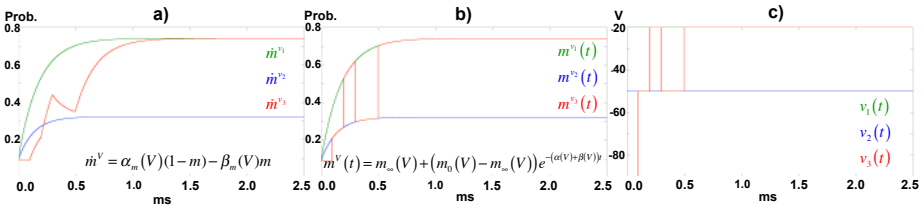

Fig. 4. Probability for the m-gate to be open in HH: a) Numerical integration of m for different voltage changes; b) Analytical solution of m for different voltage changes; c) Voltage changes applied for the analytical and the numerical integration solutions.

Then solving the DEM above as if A and B were constant and the differential equation therefore linear, Hodgkin and Huxley derived the following solution:

$$x = [m_\infty - (m_\infty - m_0)e^{-t/\tau_m}, h_\infty - (h_\infty - h_0)e^{-t/\tau_h}]'$$

As shown in Fig. 4(b) this closed-form solution jumps for a changing input shown in Fig. 4(c) between the solutions obtained for constant input. This behavior is however not problematic when replaced in the cellular model, as the voltage only jumps at the beginning, when the stimulus is applied, and then varies in a continuous way.

2.3 The IMW Sodium Current

The sodium current I_{Na} in the IMW DEM is defined by the following equation:

$$I_{Na} = \overline{g}_{Na} \left(O_1(V) + O_2(V)\right) (V - V_{Na}) \tag{2}$$

where $\overline{g}_{Na}$ and V_{Na} have the same meaning as in the HH DEM, $O_1(V)$ and $O_2(V)$ are occupancy probabilities of the two states of the MDP shown in Fig. 5.

The IMW view of the sodium channel is shown Fig. 5 [26, 28], with transition rates in Table 1. There are now four identical m-type gates, and the transition rates of the h-type gate are constant. However, these rates indirectly depend on V through the number of open-closed m gates (encoded as powers of a).

Moreover, taking the path C_0, C_1, C_1I, C_0I is mathematically equivalent to taking a voltage dependent h-transition C_0, C_0I. The longer the paths, the less one can distinguish between the HH-type and the IMW-type transition. Note also that two states O_1 and O_2 are now observable instead of one, and some bookkeeping was also added.

Definition 1. *Consider the 13-state model for sodium-channel dynamics shown in Fig. 5. Let p_j denote the j^{th} state occupancy probability from the vector* $\mathbf{p} = (C_0, C_1, C_2, C_3, C_4, O_1, O_2, C_0I, C_1I, C_2I, C_3I, C_4I, I)$. *The* ***dynamics of the model*** *M_I is described by the following system of differential equations :*

$$\frac{dp_j}{dt} = \sum_{i \neq j} k_{ij}(V) p_i - \sum_{i \neq j} k_{ji}(V) p_j \qquad i, j = 1, \ldots, 13 \tag{3}$$

where V is the transmembrane potential and $k_{ij}(V)$ is the transition rate from the i^{th} to the j^{th} state as defined in Table 1. This system can be re-written as:

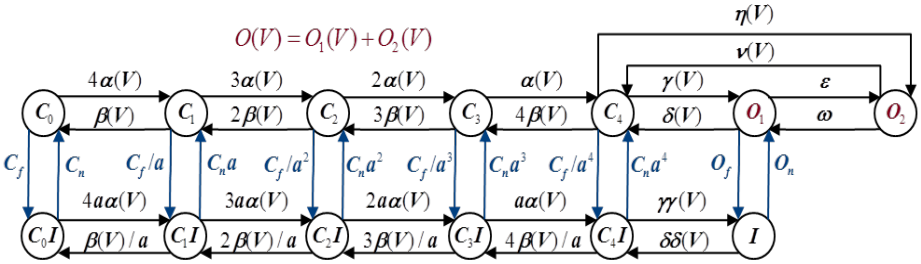

Fig. 5. The 13-variable MDP of the IMW model. The observation function is now $O = O1 + O_2$, and the transition rates of the h-type gate are constants. However, they depend on the number of open m-type gates through a. The transition rates are defined in Table 1.

$$\frac{dp_j}{dt} = A(V).\mathbf{p}, \tag{4}$$

where $A(V)$ *is a* 13×13 *matrix with* $A_{j,i}(V) = k_{ij}(V)$ $i \neq j$, $A_{j,j}(V) = -\sum_{i \neq j} k_{ji}$. *The linear system* M_{I^v} *is obtained from* M_I *by fixing* $V = v$ *in Eq. 4.*

3 Abstraction of Sodium Channel Dynamics

We construct an HH-type DEM M_H that can be substituted for M_I within the IMW cardiac-cell model. We perform the following abstractions in this process:

- We reduce the number of activating subunits to 3 and use a single inactivating subunit. This results in abstracting away the I, C_3I, C_4I, C_3 and C_4I, states of 13-state CTMDP in Figure 5.
- We coalesce the two open states into a single open state O.
- We abstract away the conditional dependence between activating and inactivating subunits of the 13-state model M_I. This is done by abstracting away the scaling factor a.
- With the above abstractions, M_I reduces to the 8-state CTMDP. The 8-state abstraction then reduces to the 2-state DEM M_H model due to the invariant manifold reduction.

Our approach to obtaining the 2-state HH-type abstraction M_H from the 13-state physiological model M_I is summarized in Fig. 6 and described next.

rate	function	rate	function	rate	function
$\alpha(V)$	$c.e^{-19.6759+0.0113V}$	$\delta\delta(V)$	$c.e^{-38.4839-0.1440V}$	ϵ	0.0227
$\beta(V)$	$c.e^{-26.2321-0.0901V}$	$\gamma\gamma(V)$	$c.e^{-21.9493+0.0301V}$	ω	1.0890
$\gamma(V)$	$c.e^{-16.5359+0.1097V}$	$\eta(V)$	$c.e^{-19.6729+0.0843V}$	c_n	0.7470
$\delta(V)$	$c.e^{-27.0926-0.0615V}$	$O_n(V)$	$c.e^{-20.6726+0.0114V}$	c_f	0.2261
$\nu(V)$	$c.e^{-26.3585-0.0678V}$	$O_f(V)$	$c.e^{-39.7449+0.0027V}$	a	1.4004

Table 1. Rates of the 13-state CT-MDP M_I shown in Fig. 5. $c = 8.513 \times 10^9$. Values instantiated from Table 6 of [20] at temperature T = 310K.

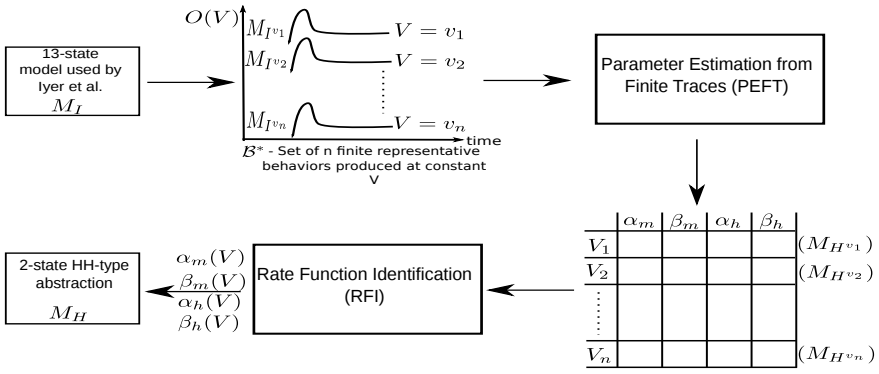

Fig. 6. Abstraction process for sodium channel dynamics.

1. **Generating representative finite traces of M_I**
   The IMW model was simulated in FORTRAN for a single cell with an integration time step of 10^{-4} ms. Multiple M_{I^v} systems were simulated for the values of V observed during the FORTRAN simulation. The linear system M_{I^v} was simulated in MATLAB using the *ODE45* solver [32]. The integration time step for these simulations was 10^{-2} ms. The simulations ran till the steady state was reached. The initial condition for all the simulations were taken to be the initial condition specified in Table 4 of [20]. The motivation for these initial conditions lies in the voltage-clamp experiments performed in [19]. In these experiments, the voltage was initially maintained at the resting potential, with the neuron conductance also being in the resting state. The voltage was suddenly increased to a specified value and the evolution of conductance was observed till steady state.
   The simulations resulted in a set $\mathcal{B}^*$, of finite-length representative behaviors (traces). Each member $\mathcal{B}^*(v)$ is the trajectory of the simulation of M_I^v.
2. **Parameter Estimation from Finite Traces (PEFT)**
   This routine takes $\mathcal{B}^*$ as the input and at each of the voltage values v, estimates the parameters of M_{H^v}, the two-state HH model (M_H) at $V = v$. For each voltage v, the following optimization problem was solved to estimate the parameters α_m^v, β_m^v, α_h^v and β_h^v of M_{H^v}:
   $$\begin{aligned} &\text{minimize} \sum_{t=0}^{t_S^v} [O^v(t) - m^v(t)^3 h^v(t)]^2 \\ &\text{subject to:} \quad \alpha_m^v, \beta_m^v, \alpha_h^v, \beta_h^v \geq 0 \end{aligned} \tag{5}$$
   where
   - t is the discrete-time step,
   - t_S^v is the number of discrete-time steps taken by M_{I^v} to reach steady state (M_{I^v} was simulated in MATLAB till steady-state),
   - $O^v(t) = O_1^v(t) + O_2^v(t)$ is the sum of the occupancy probabilities of states O_1 and O_2 in the trajectory $\mathcal{B}^*(v)$ and
   - $m^v(t)$, $h^v(t)$ define a trajectory of M_H^v:

$$
\begin{aligned}
m^v(t) &= \frac{\alpha_m^v}{\alpha_m^v + \beta_m^v} + \left(m^v(0) - \frac{\alpha_m^v}{\alpha_m^v + \beta_m^v} \right) \exp\left(- \left(\alpha_m^v + \beta_m^v \right) t \right) \\
h^v(t) &= \frac{\alpha_h^v}{\alpha_h^v + \beta_h^v} + \left(h^v(0) - \frac{\alpha_h^v}{\alpha_h^v + \beta_h^v} \right) \exp\left(- \left(\alpha_h^v + \beta_h^v \right) t \right)
\end{aligned} \tag{6}
$$

where $m^v(0)$ and $h^v(0)$ denote the initial conditions.

We used MATLAB's constrained-optimization solver *FMINCON*[33] for Eq. (5). Details of the active-set optimization algorithm implemented in the function can be found in [30]. Three aspects of our implementation deserve further elaboration:

- **Choosing $m^v(0)$ and $h^v(0)$** - In [19], the authors choose the initial conditions for all the voltages such that the inactivating gating variable h is high and the activating gating variable m is low. We use the same convention but ensure that the initial conductance (observation) $m^v(0)^3 h^v(0) = O^{V_{res}}$, where $O^{V_{res}}$ is the conductance $O_1 + O_2$ of M_I at the resting potential V_{res}. Specifically, we use $m^v(0) = 0.0026$ and $h^v(0) = 0.95$ for all v.
- **Providing seed-values** - For each voltage-value v, FMINCON needs seed values of α_m^v, β_m^v, α_h^v and β_h^v to start optimizing over the parameter space. We implemented a local search strategy for this purpose. The parameters estimated at v_i were used as seed-values for v_{i+1}. For the resting potential, when $i = 1$, the seed values were taken by evaluating Eq. (16)-(18) of [37] at $V = -90.66mV$ (the resting potential).
- **Local minima** - The solver is guaranteed to provide parameter values that locally minimize the objective function. FMINCON was run multiple times until the objective function was minimized to a value below a pre-defined threshold. The terminal values of an iteration were perturbed and used as seed-values for the next iteration. A maximum of 100 iterations were performed.

PEFT resulted in a table of parameters θ, again indexed by voltage, i.e. θ^v contained the parameters of M_{H^v}.

3. **Rate-Function Identification (RFI)**
RFI combines the parameters θ^v of M_{H^v} and outputs the parameter functions of M_H which are functions of V.This is done by identifying appropriate forms for the parameter functions $\alpha_m(V)$, $\beta_m(V)$, $\alpha_h(V)$ and $\beta_h(V)$ and then using MATLAB's curve-fitting toolbox [31] to estimate the parameters of the chosen form.

$$\alpha_m(V) = -0.6 + \frac{16.31}{1 + exp(-0.05(V + 19.67))} \tag{7}$$

$$\alpha_h(V) = \begin{cases} 0.07 + \frac{0.11}{1+exp(0.2495(V+53.01))} & V \leq -32.00 \\ 0.07 - \frac{0.06}{1+exp(-0.07(V-6.73))} & V > -32.00 \end{cases} \tag{8}$$

$$\beta_h(V) = -4.8 + \frac{145.1}{1 + exp(-0.013(V - 179))} \tag{9}$$

$$\beta_m(V) = \begin{cases} 9.92 - \frac{4.575}{1+exp(-73.73(V+63.78))} & V \leq -60.28 \\ 2.32 + \frac{2.512}{1+exp(0.2173(V+50.69))} & -60.28 < V \leq -33.04 \\ 2.26 + \frac{1.63}{1+exp(-0.2(V+20.72))} & -33.04 < V \leq -1.823 \\ -2.57 + \frac{6.73}{1+exp(0.07(V-40.23))} & V > -1.823 \end{cases} \tag{10}$$

Empirical Validation of the reduced model M_H

The 13-state model M_I was substituted by M_H in the IMW model. The modified IMW model was simulated in FORTRAN. This modified model used M_H to produce the sodium current I_{Na}. Both supra and sub-threshold stimuli, lasting for 0.5ms, were used to excite the cardiac cell. S1 and S2 denote supra-threshold stimuli of -100 pA/pF and -120 pA/pF respectively. S3 and S4 denote sub-threshold stimuli of -10 pA/pF and -20 pA/pF.

The results plotted in Fig. 7 show the behavioral equivalence of M_H and M_I. The model retains both normal and anomalous cell-level behaviors on replacing the 13-state sodium-channel component with the 2-state abstraction within the complete cell model. 2

4 Approximate Bisimulation Equivalence of M_I and M_H

We use PEFT and RFI to obtain M_H, the two-state HH-type abstraction of the 13-state model for sodium-channel dynamics M_I. We formalize the discrete-time equivalence of M_H and M_I using approximate bisimulation [15].

The approximate bisimulation relation between the state-spaces of the systems can be utilized for gaining physiological insights from formal analysis. Analysis can be done on the abstract model M_H and the results can be interpreted in the state-space of the physiological model M_I.

In [15], Pappas et al. define approximate bisimulation equivalence of Labeled Transition Systems (LTS), a generic modeling framework. We cast the models M_H and M_I as LTSs and prove approximate bisimulation equivalence of their discrete time versions. First we will establish stability properties of M_{I^v}. We use V_{res} and V_{max} to denote the resting potential and maximum potential attained at the end of the upstroke (UP) phase.

Definition 2. *A $m \times m$ square matrix M is called a closed compartmental matrix if the the following two properties are satisfied:*

1. $M_{ij} \geq 0$ *for* $i \neq j$ *- Non-diagonal entries are non-negative.*
2. $\sum_{j=1}^{n} M_{ji} = 0, \quad 1 \leq i \leq m$ *- sum of the entries in each column is 0.*

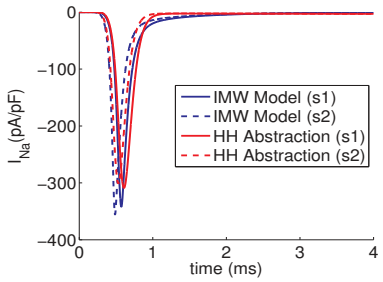

(a) Comparison of I_{Na} during the upstroke phase.

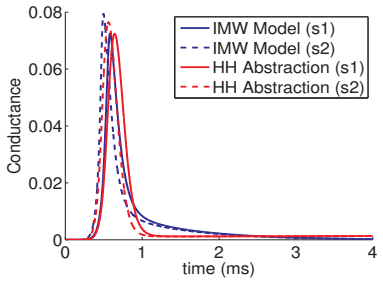

(b) Comparison of conductances ($O_1 + O_2$) of the 13-state model M_I and (m^3h) of the 2-state abstraction M_H during the upstroke phase.

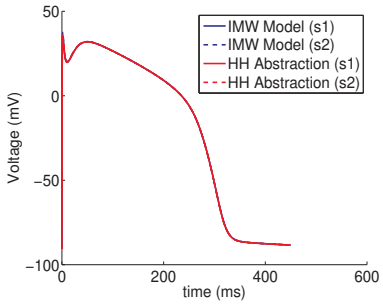

(c) Comparison of AP produced by the original IMW model and the modified version for supra-threshold stimuli.

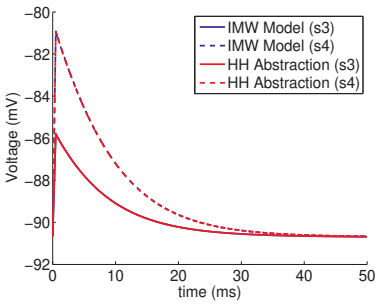

(d) Comparison of AP produced by the original IMW model and the modified version for sub-threshold stimuli.

Fig. 7. Comparison of M_I and M_H when used for I_{Na} in the IMW model. We do not show the currents and conductances for sub-threshold stimuli as they are negligible. Mean L2 errors over the duration of an AP for all stimuli: Conductance: 3.2×10^{-5}, Current: 0.1249 pA/pF, V: 0.12mV.

Lemma 1. *Let A^v be the constant matrix obtained by fixing $V = v$ in Eq. (4), where $v \in [V_{res}, V_{max}]$. A^v is a closed compartmental matrix for all $v \in [V_{res}, V_{max}]$.*

Proof. The first condition in Lemma 1 is met by construction.

For every column i, for $i \neq j$, A_{ji} is to the outgoing transition rate from state i to state j: $k_{ji}(V)$. The diagonal entry in the i^{th} column is the negated sum of all these outgoing rates, which satisfies the second condition. □

Lemma 2. *The matrix A^v, obtained by fixing $V = v$, is irreducible for all possible voltage values $v \in [V_{res}, V_{max}]$.*

Proof. A graph-theoretic proof can be made by first inducing a graph from the matrix A^v. Let $G^v(N, E)$ be the graph such that there is a node in the graph for each of the 13 states in the stochastic model in Fig. 5 and an edge $(n_i, n_j) \in E$ if and only if $A^v_{ij} \neq 0$.

Proving that G^v remains connected at all values of V, amounts to proving irreducibility of A^v. This is indeed true because of the exponential functions in Table 1. The graph G^v remains connected for all values $v \in [V_{res}, V_{max}]$. □

Theorem 1. *The model M_{I^v} has a stable equilibrium for $v \in [V_{res}, V_{max}]$.*

Proof. It follows from Proposition 4 in [21]. The prerequisites for the result are:

1. The matrix A^v must be a closed compartmental matrix.
2. The entries in A^v must be constant.
3. The matrix A^v must be irreducible.

The first condition was proved in lemma 1. The second condition holds because the rates in Table 1 are either constants or functions of V (which is fixed). We proved the third prerequisite in Lemma 2.

Proposition 4 in [21] proves that the real part of all eigenvalues of A^v is non-positive. This guarantees stability of the equilibrium. □

Theorem 1 guarantees the existence of t_S, the time taken to reach a stable steady state for $V = v$ by M_{I^v}. We proceed to cast M_I, M_H, M_{I^v} and M_{H^v} as LTSs.

Definition 3. *The LTS corresponding to M_I is the sextuple $\mathcal{I} = (X_I, \mathcal{V}, \rightarrow_I, X_I^0, \Pi_I, \langle\langle . \rangle\rangle_I)$:*

- *$X_I \subseteq \mathbb{R}^{13}$ is the **set of states** denoting the occupancy probabilities from the vector $\mathbf{p}$ in Def. 1.*
- *$\mathcal{V}$ is a family of curves (signals) of the form $[t_0, t_0 + APD] \rightarrow \mathbb{R}$ denoting **inputs** to the LTS. The lower limit t_0 is the time at which the AP commences and APD is the Action Potential Duration. $\mathcal{V}$ represents different temporal patterns by which the transmembrane potential V can be applied (fed back) to M_I, guaranteeing a solution to it. They are dictated by Eq. 1.*
- *$\rightarrow_I \subseteq X_I \times \mathcal{V} \times X_I$ is the **transition relation** that captures the dynamics of M_I such that $(\mathbf{x}_I, v, \mathbf{x}_I') \in \rightarrow_I$, written as $\mathbf{x}_I \xrightarrow{v}_I \mathbf{x}_I'$, holds when there exist $\mathcal{V} \ni v : [0, \tau] \rightarrow \mathbb{R}$ and $\xi : [0, \tau] \rightarrow \mathbb{R}^{13}$ satisfying Eq. 4 with $\xi(0) = \mathbf{x_I}$ and $\xi(\tau) = \mathbf{x_I}'$. The time taken to transit from $\mathbf{x_I}$ to $\mathbf{x_I}'$ is τ.*
- *$X_I^0 \subseteq \mathbb{R}^{13}$, a singleton consisting of the **initial condition** for M_I, is specified in Table 4 of [20] and acts as the initial state for I.*
- *$\Pi_I \subseteq \mathbb{R}$, the set of **outputs**, denotes the observable values of M_I, i.e. all possible values of $O(V) = O_1(V) + O_2(V)$, the sum of occupancy probabilities of states O_1 and O_2.*
- *$\langle\langle . \rangle\rangle_I : \mathbb{R}^{13} \rightarrow \mathbb{R}$ is the **output map**, which given a state $\mathbf{x}_I \in X_I$, maps it to its corresponding output $\pi_6(\mathbf{x}_I) + \pi_7(\mathbf{x}_I)$[6], the sum of O_1 and O_2.*

Definition 4. *The LTS corresponding to M_H is the sextuple $\mathcal{H} = (X_H, \mathcal{V}, \rightarrow_H, X_H^0, \Pi_H, \langle\langle . \rangle\rangle_H)$:*

- *$X_H \subseteq \mathbb{R}^2$ is the **set of states** denoting the values of m and h in M_H.*
- *$\mathcal{V}$, the **input set** is the same as in Def. 3. The curves $v \in \mathcal{V}$ guarantee a solution to M_H.*
- *$\rightarrow_H \subseteq X_H \times \mathcal{V} \times X_H$ is the **transition relation** that captures the dynamics of M_H such that $(\mathbf{x}_H, v, \mathbf{x}_H') \in \rightarrow_H$, written as $\mathbf{x}_H \xrightarrow{v}_H \mathbf{x}_H'$, holds when there exists curves $\mathcal{V} \ni v : [0, \tau] \rightarrow \mathbb{R}$ and $\psi : [0, \tau] \rightarrow \mathbb{R}^2$ satisfying M_H, with $\psi(0) = \mathbf{x}_H$ and $\psi(\tau) = \mathbf{x}_H'$.*

[6] $\pi_j(x)$ is the projection function that projects the j^{th} element from the vector x.

- $X_H^0 \subseteq \mathbb{R}^2$ *is a singleton consisting of the* ***initial condition*** *identified by PEFT for* $M_{H^{V_{res}}}$.
- $\Pi_H \subseteq \mathbb{R}$ *is the set of* ***outputs*** *of the LTS denoting the observables from* M_H. *As* I_{Na} *current depends on the conductance* m^3h *of* M_H, *the set* Π_H *contains all possible values of* m^3h.
- $\langle\langle . \rangle\rangle_H : \mathbb{R}^2 \to \mathbb{R}$ *is the* ***output map****, which given a state* $\mathbf{x}_H \in X_H$, *maps it to its corresponding output* $(\pi_1(\mathbf{x}_H))^3\pi_2(\mathbf{x}_H)$, *the conductance* m^3h.

Definition 5. *The LTS corresponding to* M_{I^v} *is the sextuple* $\mathcal{I}^v = (X_{I^v}, T, \rightarrow_{I^v}, X^0_{I^v}, \Pi_{I^v}, \langle\langle . \rangle\rangle_{I^v})$. *The states* X_{I^v}, *outputs* Π_{I^v} *and output map* $\langle\langle . \rangle\rangle_{I^v}$ *are the same as in Def. 3.*

- $T \subseteq \mathbb{R}_{\geq 0}$ *is the* ***input****, denoting time.*
- $\rightarrow_{I^v}$ *is the* ***transition relation*** *such that* $\mathbf{x}_{I^v} \xrightarrow{t}_{I^v} \mathbf{x}'_{I^v}$ *holds if there exists a solution* ξ^v *to* M_{I^v} *satisfying* $\xi^v(0) = \mathbf{x}_{I^v}$ *and* $\xi^v(t) = \mathbf{x}'_{I^v}$.
- $X^0_{I^v}$ *denotes the* ***initial condition*** *used in step 1 of the three-step procedure in Section 3.*

Definition 6. *The LTS corresponding to* M_{H^v} *is the sextuple* $\mathcal{H}^v = (X_{H^v}, T, \rightarrow_{H^v}, X^0_{H^v}, \Pi_{H^v}, \langle\langle . \rangle\rangle_{H^v})$. *The states* X_{H^v}, *outputs* Π_{H^v} *and output map* $\langle\langle . \rangle\rangle_{H^v}$ *are the same as in Def. 4. The input set* T *is the same as in Def. 5.*

- $\rightarrow_{H^v}$ *is the* ***transition relation*** *such that* $\mathbf{x}_{H^v} \xrightarrow{t}_{H^v} \mathbf{x}'_{H^v}$ *holds if there exists a solution* ψ^v *to* M^v_H *satisfying* $\psi^v(0) = \mathbf{x}_{H^v}$ *and* $\psi^v(t) = \mathbf{x}'_{H^v}$.
- $X^0_{H^v}$ *is the* ***initial condition*** *determined by PEFT in Sec 3 for* $V = v$.

Definition 7. *The two LTSs* $T_1(Q_1, \Sigma, \rightarrow_1, Q_1^0, \Pi, \langle\langle . \rangle\rangle_1)$ *and* $T_2(Q_2, \Sigma, \rightarrow_2, Q_2^0, \Pi, \langle\langle . \rangle\rangle_2)$ *are approximately bisimilar, with precision* δ, *denoted as* $T_1 \cong_\delta T_2$, *if there exists a relation* $B_\delta \subseteq Q_1 \times Q_2$ *such that:*

1. *For every* $q_1 \in Q_1^0$, *there exists a* $q_2 \in Q_2^0$ *such that* $(q_1, q_2) \in B_\delta$ *and conversely.*
2. *For every* $(q_1, q_2) \in B_\delta$, $d_\Pi(\langle\langle q_1 \rangle\rangle_1, \langle\langle q_2 \rangle\rangle_2) \leq \delta$, *where* d_Π *is some distance metric defined on the output set* Π *shared by the two LTS.*
3. *For every* $(q_1, q_2) \in B_\delta$*:*
   (a) $q_1 \xrightarrow{\sigma}_1 q'_1$, $\sigma \in \Sigma$, *implies the existence of* $q_2 \xrightarrow{\sigma}_2 q'_2$ *such that* $(q'_1, q'_2) \in B_\delta$.
   (b) $q_2 \xrightarrow{\sigma}_2 q'_2$, $\sigma \in \Sigma$, *implies the existence of* $q_1 \xrightarrow{\sigma}_1 q'_1$ *such that* $(q'_1, q'_2) \in B_\delta$.

The relation B_δ *is called the approximate bisimulation relation.*

In the case of deterministic systems, such as $\mathcal{I}$, $\mathcal{H}$, $\mathcal{I}^v$ and $\mathcal{H}^v$, proving two LTSs approximately bisimilar is equivalent to proving that the distance between the unique trajectories (behaviors) of the systems is bounded. Next, we state a simple lemma relating finite-length trajectories of two Linear Autonomous Dynamical Systems (LADS)[7], whose proof follows from the uniqueness and continuity of the trajectories.

[7] See Lecture 9 of [3] for a formal definition of LADS.

Lemma 3. *Consider two LADSs* $\{\dot{\mathbf{x}}_1 = M_1.\mathbf{x}_1,\ \mathbf{x}_1(0) = \mathbf{x}_1^0\}$ *and* $\{\dot{\mathbf{x}}_2 = M_2.\mathbf{x}_2,\ \mathbf{x}_2(0) = \mathbf{x}_2^0\}$ *where* $\mathbf{x}_1, \mathbf{x}_2, \mathbf{x}_1^0, \mathbf{x}_2^0 \in \mathbb{R}^n$ *and* M_1 *and* M_2 *are* $n \times n$ *matrices. Let* $\mathbf{x}_1(t)$ *and* $\mathbf{x}_2(t)$ *be the respective solution trajectories. Let* $I_1[t_1, t_2]$ *and* $I_2[t_2, t_3]$ *be two time intervals of arbitrary lengths such that:*

- $|\mathbf{x}_1(t) - \mathbf{x}_2(t)| \leq \delta$ *for* $t \in I_1$, *and*
- $|\mathbf{x}_1(t) - \mathbf{x}_2(t)| \leq \delta$ *for* $t \in I_2$,

where $|.|$ *denotes the L2 norm. Then* $|\mathbf{x}_1(t) - \mathbf{x}_2(t)| \leq \delta$ *for* $t \in I_{12}[t_1, t_3]$.

Definition 8. *The LTSs* $\mathcal{I}_d$, $\mathcal{H}_d$, $\mathcal{I}_d^v$ *and* $\mathcal{H}_d^v$ *denote discrete time equivalents of the LTSs* $\mathcal{I}$, $\mathcal{H}$, $\mathcal{I}^v$ *and* $\mathcal{H}^v$ *respectively such that:*

- *The input curves* v *for* $\mathcal{I}_d$ *and* $\mathcal{H}_d$ *are discrete time signals of voltage of the the form* $[v_1, v_2, \ldots, v_i, \ldots]$, *where* v_i *is the voltage at the* i^{th} *time step. The inputs to* $\mathcal{I}_d^v$ *and* $\mathcal{H}_d^v$ *are integral multiples of the time step.*
- *The transition relations of the LTSs respect the transitions of the corresponding continuous time ones, except that the dynamics are now defined in discrete time. Chapter 11 of [27] provides details about converting continuous time models to discrete time versions via techniques like sample and hold.*

Note: Discrete time arguments can be justified because the LADS resulting at constant voltages are band-limited as they attain steady state in finite time for all voltages (see Theorem 1). For such systems, the Sampling theorem [27] guarantees the existence of a Digital to Analog Converter (DAC) that can recover the continuous time behaviors from discrete time samples, if a small-enough discretization of time is used. This sampling frequency is determined by the maximum frequency component in the continuous-time behaviors. Theorem 1 ensures that the maximum frequency component of the trajectories is bounded for all voltages.

Theorem 2. *The PEFT procedure can ensure that* $\mathcal{I}_d^v \cong_{\delta^v} \mathcal{H}_d^v$ *for any* $v \in [V_{res}, V_{max}]$. *The precision* δ^v *is the maximum L2 error incurred by the optimizer while solving Eq. (5).*

Proof The approximate bisimulation relation $B_{\delta^v} \subseteq X_{I^v} \times X_{H^v}$ can be constructed as follows.

1. The initial condition in $\mathbf{x}_{I^v}^0 \in X_{I^v}^0$ is paired with the initial condition $\mathbf{x}_{H^v}^0 \in X_{H^v}^0$.
2. Consider a state $\mathbf{x}_{I^v} \in X_{I^v}$ such that $\mathbf{x}_{I^v}^0 \xrightarrow{t}_{I^v} \mathbf{x}_{I^v}$, $t \in T$. Also say $\mathbf{x}_{H^v} \in X_{H^v}$ such that $\mathbf{x}_{H^v}^0 \xrightarrow{t}_{H^v} \mathbf{x}_{H^v}$. Then, $(\mathbf{x}_{I^v}, \mathbf{x}_{H^v}) \in B_{\delta^v}$. The existence of states $\mathbf{x}_{I^v}$ and $\mathbf{x}_{H^v}$ satisfying the conditions is guaranteed due to uniqueness and existence of solutions to LADS.

The relation B_{δ^v} is a valid approximate bisimulation relation. Condition 1 of Def. 7 is satisfied by construction. Suppose we have $(\mathbf{x}_{I^v}, \mathbf{x}_{H^v}) \in B_{\delta^v}$, $\mathbf{x}_{I^v} \xrightarrow{t'}_{I^v} \mathbf{x}'_{I^v}$, and $\mathbf{x}_{H^v} \xrightarrow{t'}_{H^v} \mathbf{x}'_{H^v}$, then we have $\mathbf{x}_{I^v}^0 \xrightarrow{t+t'}_{I^v} \mathbf{x}'_{I^v}$ and $\mathbf{x}_{H^v}^0 \xrightarrow{t+t'}_{H^v} \mathbf{x}'_{H^v}$, due to the uniqueness of the trajectories, where t is the time required to transit

from $\mathbf{x}^0_{I^v}$ to $\mathbf{x}_{I^v}$ and from $\mathbf{x}^0_{H^v}$ to $\mathbf{x}_{H^v}$ in $\mathcal{I}^v_d$ and $\mathcal{H}^v_d$ respectively. This ensures that $(\mathbf{x}'_{I^v}, \mathbf{x}'_{H^v}) \in B_{\delta^v}$, thus satisfying condition 2 of Def. 7. Condition 3 is satisfied due to Lemma 3, which also holds for discrete time trajectories. □

We now define perturbed LADS. Then we outline the approximate bisimilarity of $\mathcal{I}_d$ and $\mathcal{H}_d$.

Definition 9. *Consider an LADS* $\{\dot{\mathbf{x}} = M.\mathbf{x},\ \mathbf{x}(0) = \mathbf{x}^0\}$*, where* $\mathbf{x}, \mathbf{x}^0 \in \mathbb{R}^n$*,* M *is a* $n \times n$ *matrix and* $\mathbf{x}(0)$ *is the initial condition. An* ϵ*-perturbation of the LADS is obtained by perturbing any of the entries in* M *or* $\mathbf{x}(0)$ *by at-most* $\epsilon \in \mathbb{R}$*.*

Theorem 3. *The three-step abstraction process explained in Section 3 ensures that* $\mathcal{H}_d \cong_\delta \mathcal{I}_d$ *with* $\delta \leq 7.58 \times 10^{-4}$*.*

Proof sketch: In discrete time, the evolution of M_H (M_I) can be modeled as a series of one-step evolutions of M_{H^v} (M_{I^v}) i.e. when the input signal is of the form $[v_1, \ldots, v_i, v_{i+1} \ldots]$, at the i^{th} step, the LADS $M_{H^{v_i}}$ $(M_{I^{v_i}})$ evolves for one time step, followed by $M_{H^{v_{i+1}}}$ $(M_{I^{v_{i+1}}})$ and so on. This idea is also illustrated in Fig. 4(b).

For some voltage $V = v$, the distance between the trajectories of M_{I^v} and M_{H^v} can be bound in terms of the trajectories of $M_{I^{v^*}}$ and $M_{H^{v^*}}$, where v^* is a voltage that was processed by PEFT and M_{I^v} is a minimal perturbation of $M_{I^{v*}}$. At the i^{th} step, the perturbation is the least for $M_{I^{v^*_i}}$ among all the voltages that were processed by PEFT. We first bound the corresponding perturbation of $M_{H^{v_{i^*}}}$, ϵ, and then use a similar approach for $M_{I^{v^*_i}}$
$\epsilon = max(\epsilon_1, \epsilon_2)$,where

$$\epsilon_1 = \max_{1 \leq j \leq n} [max\{|\alpha_m(v_j) - \alpha_m(v_{j+1})|, |\beta_m(v_j) - \beta_m(v_{j+1})|, |\alpha_h(v_j) - \alpha_h(v_{j+1})|, |\beta_h(v_j) - \beta_h(v_{j+1})|\}],$$

$$\epsilon_2 = max[|\alpha_m(v_\Delta) - \alpha_m(v_{\Delta+1})|, |\beta_m(v_\Delta) - \beta_m(v_{\Delta+1})|, |\alpha_h(v_\Delta) - \alpha_h(v_{\Delta+1})|, |\beta_h(v_\Delta) - \beta_h(v_{\Delta+1})|]$$

and $\Delta = \underset{1 \leq j \leq n}{\text{argmax}}[\frac{|v_j - v_{j+1}|}{2}]$

The limit n is the total number of voltages processed by PEFT. The term ϵ_1 accounts for sharp changes in the rate functions $\alpha_m(V)$, $\alpha_h(V)$, $\beta_m(V)$, $\beta_h(V)$ and ϵ_2 accounts for sparsity in the voltages processed by PEFT. Given the input signal v, the i^{th} step v_i may be at most Δ mV away from a voltage processed by PEFT.

At the i^{th} step, let $M_{H^{v_i}}$ be an ϵ-perturbation of $M_{H^{v^*_i}}$ and at the $(i+1)^{th}$ step, let $M_{H^{v_{i+1}}}$ be an ϵ-perturbation of $M_{H^{v^*_{i+1}}}$. We can always ensure that $v^*_i \neq v^*_{i+1}$. This can be done by first bounding the time-scale, which determines the maximum change in V that can occur over one time step, $(|v_i - v_{i+1}|)$. Once we know the least value of $|v_i - v_{i+1}|$, we can perform the PEFT procedure for voltages that satisfy $\Delta \leq |v_i - v_{i+1}|$. Thus, we can ensure that at the i^{th} step, the perturbed-system $M_{H^{v_i}}$ $(M_{I^{v_i}})$ diverges from $M_{H^{v^*_i}}$ $(M_{I^{v^*_i}})$ for at most one time step.

We first bound the one-step divergence between the trajectories of $M_{H^{v_i}}$ and $M_{H^{v_i^*}}$. We calculate the sensitivity of the variable m to an ϵ change in the parameters and the initial conditions below.

$$\begin{aligned}
\dot{m}^{v_i^*} &= \alpha_m^{v_i^*}(1-m) + \beta_m^{v_i^*} m \\
m^{v_i^*}[1] &= m_0^{v_i^*} + [\alpha_m^{v_i^*}(1-m_0^{v_i^*}) + \beta_m^{v_i^*} m_0^{v_i^*}] \quad \text{(one time step)} \\
m^{v_i}[1] &= m_0^{v_i^*} + \epsilon + [(\alpha_m^{v_i^*}+\epsilon)(1-m_0^{v_i^*}) + (\beta_m^{v_i^*}+\epsilon) m_0^{v_i^*}] \text{(perturbed)} \\
|m^{v_i^*}[1] - m^{v_i}[1]| &= |\epsilon[1 + (1 - 2m - \alpha_m^{v_i} - 2\epsilon - \beta_m^{v_i})]| \quad \text{(divergence)} \\
&\leq |2\epsilon|
\end{aligned}$$

The divergence is maximized when $m = 0$ and the transition rates $\alpha, \beta = 0$. Thus given an initial separation of ϵ, the trajectories diverge by at most 2ϵ in one time-step. The same calculation can be repeated independently for h.

Theorem 2 dictates that the trajectories of $M_{I^{v_i^*}}$ and $M_{H^{v_i^*}}$ may not diverge beyond $\delta^{v_i^*}$. This is implied by their approximate bisimulation equivalence.

Using a similar approach as taken for $M_{H^{v_i}}$, we now bound the divergence of trajectories of $M_{I^{v_i}}$ from $M_{I^{v_i^*}}$. At $V = v_i$, the maximum possible perturbation μ of $M_{I^{v_i}}$ from $M_{I^{v_i^*}}$, where v_i^* is the nearest voltage processed by PEFT, can be bound as was done for ϵ, by considering the rate functions of M_I. The solution trajectory of $M_{I^{v_i^*}}$ is given by the matrix exponential $e^{A(v_i^*)t}$, where A is the matrix in Eq.(4). An arbitrary voltage v_i in the input-signal presents a μ-perturbation of the entries in $A(v_i^*)$. The evolution of $M_{I^{v_i}}$ is then approximated by the corresponding perturbation of $e^{A(v_i^*)t}$.

The matrix exponential is determined by the eigenvalues of $A(v_i^*)$. Bauer-Fike theorem [2] bounds the spectral perturbation caused due to a perturbation of the original matrix. It ensures that the eigenvalues of $A(v_i)$ are μ-perturbations of the eigenvalues of $A(v_i^*)$. Thus, the maximum divergence[8] of $M_I^{v_i}$ from $M_I^{v_i^*}$ in one time-step is at most e^μ.

Thus, $\delta \leq 16\epsilon^4 + \underset{1\leq i\leq n}{\text{argmax}}[\delta^{v_i^*}] + e^\mu$, sum of the following quantities:

- Maximum divergence of $M_{H^{v_i}}$ from $M_{H^{v_i^*}}$ over one time-step: $16\epsilon^4$. This is due to the conductance being m^3h. We bound the divergence of m and h individually at 2ϵ.
- Maximum divergence of any $M_{H^{v_i^*}}$ from $M_{I^{v_i^*}}$ over all n voltages processed during PEFT: $\underset{1\leq i\leq n}{\text{argmax}}[\delta^{v_i^*}]$. This was estimated to be 2.79×10^{-4}.
- Maximum divergence of $M_{I^{v_i}}$ from $M_{I^{v_i^*}}$ over one time step: e^μ. □

5 Related Work

Singular perturbation [24, 34] and invariant manifold reduction [6, 16] are two popular approaches to reducing multi-scale state-space models of chemical reaction kinetics [7, 17, 38]. The quasi steady state assumption is central to singular perturbation techniques used in [38]. The derivative of fast variables, which

[8] A tighter bound can be found, as was done for $M_{H^{v_i}}$, by projecting the error onto the O_1 and O_2 dimensions.

evolve on relatively short time scales, is approximated to be zero, resulting in model reduction. Despite being successful for chemical kinetics models, such techniques are not well-suited for Markovian ion channel models. The former involves a constant rate matrix A that renders the system linear, where as in our Markovian models, the rate matrix A is a function of the transmembrane voltage V. The voltage V is itself dependent on the evolution of the Markovian model and this circular dependency causes the overall model to be nonlinear.

Reduction of Markovian ion-channel models, which is the central topic of this paper, has been explored in [41, 42]. The focus is on reducing the simulation time, rather than obtaining a formal reduction. In [39] Smith et al. reduce a stochastic model for the sodium-potassium pump by lumping the states of their model. In [10], Fink et al. use mixed formulations of an HH-type model and a Markovian model to reduce the number of state variables for the calcium current. In this paper, we provide a systematic reduction of the sodium channel. Conventional approaches like [25] use behavioral equivalence to validate the reduced models. Approximate bisimulation, used in this paper, formalize equivalence in a compositional setting and also help in insightful analysis.

6 Conclusions and Future Work

We constructed a two-state Hodgkin-Huxley-type model M_H that can replace the 13-state CT-MDP M_I for sodium-channel dynamics, within the IMW model for ventricular myocytes. The open state of M_I being the only observable was an underlying assumption in the reduction. It should be noted that this is not very restrictive. Any observable state occupancy probability can be handled by modifying Eq. (5). Currently we map the open state probabilities of M_I and the 8-state CT-MDP in Fig. 3 to each other. Once such a mapping is established between any two states of the two models, Eq. (5) can then be modified to fit the trajectories of the states of M_I that one is interested in. The invariant manifold of the m and h is related to all the 8 states.

The reduction was formalized by proving the abstract and the concrete models to be approximately bisimilar. This notion of system equivalence can be used for compositional reasoning. When $\mathcal{H}$ is appropriately composed with the rest of the larger whole-cell IMW model, approximate bisimulation guarantees that the newly composed-system retains the properties of the original system. The original system can be modeled as an appropriate composition of $\mathcal{I}$ and rest of the IMW model. In the future, further complicated non-deterministic models will be explored and reduced. Tighter bounds will also be pursued for the precision of the bisimulation relation. We then plan to use the *towers of abstraction* constructed from the strategy outlined in the paper, for insightful analysis of cardiac models.

References

1. E. Bartocci, E. Cherry, J. Glimm, R. Grosu, S. A. Smolka, and F. Fenton. Toward real-time simulation of cardiac dynamics. In *Proceedings of the 9th Inter-*

national Conference on Computational Methods in Systems Biology, CMSB'2011, pages 103–112. ACM, 2011.
2. F. L. Bauer and C. T. Fike. *Norms and Exclusion Theorems*. Numerische Matematik, 1960.
3. S. Boyd. *EE 263: Introduction to Linear Dynamical Systems, lecture notes*. Stanford Engineering Everywhere (SEE), 2010.
4. A. Bueno-Orovio, E. M. Cherry, and F. H. Fenton. Minimal model for human ventricular action potentials in tissue. *J. of Theor. Biology*, 253(3):544–560, 2008.
5. E. M. Cherry and F. H. Fenton. Visualization of spiral and scroll waves in simulated and experimental cardiac tissue. *New Journal of Physics*, 10:125016, 2008.
6. E. Chiavazzo, A. N. Gorban, and I. V. Karlin. Comparisons of invariant manifolds for model reduction in chemical kinetics. *Comm Comp Phys*, 2:964 –992, 2007.
7. I. R. Epstein and J. A. Pojman. *An Introduction to Nonlinear Chemical Dynamics*. Oxford University Press, London, 1998.
8. F. Fenton and A. Karma. Vortex dynamics in three-dimensional continuous myocardium with fiber rotation: Filament instability and fibrillation. *Chaos*, 8(1):20–47, 1998.
9. F. H. Fenton and E. M. Cherry. Models of cardiac cell. *Scholarpedia*, 3:1868, 2008.
10. M. Fink and D. Noble. Markov models for ion channels: Versatility versus identifiability and speed. *Philosophical Transactions of the Royal Society A: Mathematical, Physical and Engineering Sciences*, 367(1896):2161–2179, 2009.
11. J. Fisher, N. Piterman, and M. Y. Vardi. The only way is up. In *Proceedings of the 17th international conference on Formal methods*, FM'11, pages 3–11, Berlin, Heidelberg, 2011. Springer-Verlag.
12. A. Girard. Controller synthesis for safety and reachability via approximate bisimulation. *Automatica*, 48:947–953, 2012.
13. A. Girard and G. J. Pappas. Approximate bisimulations for nonlinear dynamical systems. In *Proc. of CDC'05, the 44th Int. Conf. on Decision and Control*, Seville, Spain, December 2005. IEEE.
14. A. Girard and G. J. Pappas. Approximate bisimulation relations for constrained linear systems. *Automatica*, 43:1307–1317, 2007.
15. A. Girard and G. J. Pappas. Approximation metrics for discrete and continuous systems. *Automatic Control, IEEE Transactions on*, 52(5):782 –798, May 2007.
16. A. N. Gorban and I. V. Karlin. Method of invariant manifold for chemical kinetics. *Chem. Eng. Sci.*, 58:4751 –4768, 2003.
17. A. N. Gorban, N. Kazantzis, I. G. Kevrekidis, H. C. Ottinger, and C. Theodoropoulos. *Model reduction and coarse-graining approaches for multiscale phenomena*. Springer, 2006.
18. R. Grosu, G. Batt, F. Fenton, J. Glimm, C. L. Guernic, S. A. Smolka, and E. Bartocci. From cardiac cells to genetic regulatory networks. In *Proc. of CAV'11, the 23rd International Conference on Computer Aided Verification*, LNCS, Cliff Lodge, Snowbird, Utah, USA, July 2011. Springer.
19. A. L. Hodgkin and A. F. Huxley. A quantitative description of membrane current and its application to conduction and excitation in nerve. *Journal of Physiology*, 117:500–544, 1952.
20. V. Iyer, R. Mazhari, and R. L. Winslow. A computational model of the human left-ventricular epicardial myocytes. *Biophysical Journal*, 87(3):1507–1525, 2004.
21. T. Jahnke and W. Huisinga. Solving the chemical master equation for monomolecular reaction systems analytically. *Journal of Mathematical Biology*, 54:1–26, July 2007.

22. Jasmin Fisher, David Harel, and Thomas A. Henzinger. Biology as reactivity. *Communications of the ACM*, 54(10):72–82, October 2011.
23. J. Keener. Invariant manifold reductions for markovian ion channel dynamics. *Journal of Mathematical Biology*, 58(3):447–457, July 2009.
24. J. Kevorkian and J. D. Cole. *Multiple Scale and Singular Perturbation Methods*. Springer-Verlag, 1996.
25. P. Kienker. Equivalence of aggregated markov models of ion-channel gating. *Proceedings of the Royal Society of London. B. Biological Sciences*, 236(1284):269–309, 1989.
26. C.-C. Kuo and B. P. Bean. Na channels must deactivate to recover from inactivation. *Neuron*, 12:819–829, 1994.
27. E. Lee and P. Varaiya. *Structure and Interpretation of Signals and Systems*. Pearson Education, 2003.
28. Lisa A. Irvine, M. Saleet Jafri, and Raimond L. Winslow. Cardiac sodium channel markov model with tempretature dependence and recovery from inactivation. *Biophysical Journal*, 76:1868–1885, 1999.
29. C. H. Luo and Y. Rudy. A dynamic model of the cardiac ventricular action potential. I. Simulations of ionic currents and concentration changes. *Circulation Research*, 74(6):1071–1096, June 1994.
30. MATLAB. Choosing a solver. www.mathworks.com/help/toolbox/optim.
31. MATLAB. Curve fitting toolbox. www.mathworks.com/products/curvefitting.
32. MATLAB. Nonlinear numerical methods. www.mathworks.com/help/techdoc/ref/f16-5872.html.
33. MATLAB. Optimization toolbox. http://www.mathworks.com/help/toolbox/optim.
34. J. D. Murray. *Mathematical Biology*. Springer-Verlag, 1990.
35. C. J. Myers. *Engineering Genetic Circuits*. CRC Press, 2010.
36. National Science Foundation (NSF). Computational Modeling and Analysis of Complex Systems (CMACS). http://cmacs.cmu.edu.
37. D. Noble. A modification of the Hodgkin-Huxley equations applicable to purkinje fibre action and pace-maker potentials. *J. Physiol.*, 160:317–352, 1962.
38. O. Radulescu, A. N. Gorban, A. Zinovyev, and A. Lilienbaum. Robust simplifications of multiscale biochemical networks. *BMC Systems Biology*, 2(1):86, 2008.
39. N. Smith and E. Crampin. Development of models of active ion transport for whole-cell modelling: Cardiac sodium-potassium pump as a case study. *Progress in Biophysics and Molecular Biology*, 85(23):387 – 405, 2004. Modelling Cellular and Tissue Function.
40. K. H. ten Tusscher, D. Noble, P. J. Noble, and A. V. Panfilov. A model for human ventricular tissue. *American Journal of Physiology*, 286:H1573–H1589, 2004.
41. C. Wang, P. Beyerlein, H. Pospisil, A. Krause, C. Nugent, and W. Dubitzk. An efficient method for modeling kinetic behavior of channel proteins in cardiomyocytes. *IEEE/ACM Trans. on Computational Biology and Bioinformatics*, 9(1):40–51, Jan/Feb 2012.
42. J. P. Whiteley. Model reduction using a posteriori analysis. *Mathematical Biosciences*, 225(1):44 – 52, 2010.